A Compressed Sampling for Spherical Near-Field Measurements

Cosme Culotta-López, Dirk Heberling
Institute of High Frequency Technology
RWTH Aachen University
Germany
{culotta, heberling}@ihf.rwth-aachen.de

Arya Bangun, Arash Behboodi, Rudolf Mathar
Institute for Theoretical Information Technology
RWTH Aachen University
Germany
{bangun, behboodi, mathar}@ti.rwth-aachen.de

Abstract—**Spherical near-field measurements are regarded as the most accurate technique for the characterization of an Antenna Under Tests (AUT) radiation. The AUT's far-field radiation characteristics can be calculated from the Spherical Mode Coefficients (SMC), or spherical wave coefficients, determined from near-field data. The disadvantage of this technique is that, for the calculation of the SMC, a whole sphere containing the AUT must be Nyquist-sampled, thus directly implying a longer measurement time when only a few cuts are of interest. Due to antennas being spatially band-limited, they can be described with a finite number of SMC. Besides, the vector containing the SMC can be proved sparse under certain circumstances, e.g., if the AUT's radiation pattern presents information redundancy, such as an electrical symmetry with respect to coordinate system of the measurement. In this paper, a novel sampling strategy is proposed and is combined with compressed-sensing techniques, such as basis pursuit solvers, to retrieve the sparse SMC. The retrieved sparse SMC are then used to obtain the AUT's far-field radiation. The resulting far-field pattern is compared for both simulated and measured data. The reduced number of points needed for the presented sampling scheme is compared with classical equiangular sampling, together with the estimated acquisition time. The proposed sampling scheme improves the acquisition time with a reasonable error.**

I. Introduction

In the decade of the 1980s, efforts were made to reduce the spatial requirements for antenna measurements and to allow three-dimensional measurements in the AUT's near field [1], [2]. Decomposing the measured data in near field in a weighted superposition of spherical waves, called spherical harmonics (SH) and closely related to the Wigner-D basis, it is possible to calculate their superposition at any point in space knowing only its weighting coefficients, also called the Spherical Mode Coefficients (SMC). This allows for the calculation of the pattern at an infinite distance from the AUT, that is, the far-field pattern. This approach requires smaller measurement chambers and relegates part of the measurement process to the nowadays comparatively cheap computational chain, thus reducing the potential measurement costs. However, a whole sphere must be sampled for the SMC to be calculated, which leads to a longer measurement time if only some part of the radiation pattern is of interest.
To further sink the costs of antenna measurements, one current approach is to reduce the measurement time. Efforts have been made to find more efficient sampling strategies than the classical equiangular sampling [3], [4], which Nyquist-samples the sphere on its equator and oversamples it on every other cut, leading to the development of alternative SMC calculation methods that allow to sample a different number of points in each cut [5]–[7]. Another approach is to take advantage of the inherent sparsity of the SMC, i.e., of a large part of the terms being zero under certain conditions, to undersample the sphere and still be able to reconstruct the radiation pattern using compressed-sensing solvers. The intention is, by acquiring a reduced number of points, to save measurement time and thus to improve the efficiency of measurement chambers. Current research in this field [8]–[10] proves it possible to retrieve the radiation information from a set of undersampled measurements. However, the suggested sampling strategies do not normally reduce the number or the length of the movements a conventional roll-over-azimuth positioner performs in a measurement. Thus, these strategies do not reduce the measurement time in conventional cases and are only of interest for measurements where the acquisition equipment itself limits the antenna positioner's speed.

In this paper, a novel undersampled sampling scheme that minimizes the coherence of the sampling matrix is introduced. The SMC are reconstructed with compressed-sensing techniques from simulation and measurement data, sampled with the proposed method. The SH decomposition is explained in Section II, together with the sparsity assumption and the applied definition of phase center. In Section III, the proposed sampling scheme is introduced and explained. In Section IV, results for simulated noiseless data are shown, whereas in Section V results for real measurements are discussed, with a focus on the saved measurement time. Section VI sums up the conclusions and suggests paths for future work.

II. Theoretical Background

In this section, the Spherical Wave Expansion (SWE) is discussed. The electromagnetic field on the surface of a sphere enclosing a radiating object can be expressed using the SWE, which is used as framework for Spherical Near-Field (SNF) antenna measurements [1]. Moreover, as discussed in [7], [10], the SWE can be represented as a system of linear equations of the type $y = Ax$, in which the performance of the sensing or sampling matrix A depends on the sampling pattern over

the sphere.

The general probe-corrected transmission formula [1] can be expressed as

$$w(A, \chi, \theta, \phi) =$$
$$= \sum_{s=1}^{2} \sum_{\mu=-\nu_{\max}}^{\mu=\nu_{\max}} \sum_{l=1}^{\infty} \sum_{m=-l}^{l} T_{slm} D_{\mu m}^{l}(\theta, \phi, \chi) P_{s\mu l}(kA), \quad (1)$$

where $w(A, \chi, \theta, \phi)$ is the measurement signal at the distance A, polarization angle χ and rotation angles θ and ϕ, T_{slm} are the SMC, or in this notation transmission coefficients, the product $D_{\mu m}^{l}(\theta, \phi, \chi) = e^{jm\phi} d_{\mu m}^{l}(\theta) e^{j\mu\chi}$ represents the Euler rotation of spherical waves, also called Wigner D-functions, and $P_{s\mu l}(kA)$ is the probe response constant.

Since antennas are band limited, the summation over l can be truncated to the band-limit constant B, so that $1 \leq l \leq B$, thus also making the summation over m, $-l \leq m \leq l$, finite. This upper band limit is described by

$$B = kr_0 + L_0, \quad (2)$$

where k is the wavenumber, r_0 is the radius of the minimum sphere containing the AUT and L_0 is a constant used for stability and accuracy. In the literature, the choice of $L_0 = 10$ is frequently supported. Higher order modes do also propagate but are highly attenuated and their contribution to the far-field radiation pattern is limited. At the same time, s is limited to the values 1 and 2, one of them representing the propagation of TE modes and, the other one, the propagation of TM modes. The radiated power can be calculated from the transmission coefficients as

$$P_{\text{rad}, \bar{r}} = \frac{1}{2} \sum_{slm} |T_{slm, \bar{r}}|^2 = \frac{1}{2} \sum_{s=1}^{2} \sum_{l=1}^{B} \sum_{m=-l}^{l} |T_{slm, \bar{r}}|^2. \quad (3)$$

With these conditions, the total number of modes N is calculated by

$$N = 2B(B+2) = 2B^2 + 4B. \quad (4)$$

The general probe-corrected transmission formula can be represented as a matrix equation:

$$\boldsymbol{w} = \boldsymbol{\Psi} \boldsymbol{q}, \quad (5)$$

with $\boldsymbol{w} \in \mathbb{C}^M$ as the measurement signal vector, $\boldsymbol{\Psi} \in \mathbb{C}^{M \times N}$ as the matrix containing the sample of Euler rotation or Wigner-D functions and probe response constant and $\boldsymbol{q} \in \mathbb{C}^N$ as the antenna transmission coefficient vector. For this system and taking into account the aforementioned considerations, a total of $M = N$ measurements suffice to solve the linear equation system. However, the typical equiangular sampling delivers a total number of samples of

$$M = M_\chi M_\theta M_\phi = 2(B+1)(2B+1) =$$
$$= 4B^2 + 6B + 2 > 2N, \quad (6)$$

being almost twice the strictly required samples. Many equiangular sampling points being linearly dependent further contributes to the inefficiency of this sampling strategy. However,

this sampling does deliver a well-conditioned problem [7]. The scope of this paper is to reduce the number of measurements $M < N$ for radiating objects with sparse or compressible SMC.

A. Phase Center and Sparsity

As mentioned in [11], the sparsity of the coefficient vector T_{slm} does not only depend on the AUT but also on the coordinate system chosen for the expansion. This implies that the geometrical properties of the AUT, its radiated field and the relationship to the chosen expansion's coordinate system directly influence the coefficients vector T_{slm}. Having the SH definite parity i.e being either even or odd with respect to inversion about the origin, it can be assumed that, given an AUT radiating a field with any type of symmetry, a solution where less terms of T_{slm} are required for the AUT's complete description exists. It is assumed this solution is found when the expansion's coordinate system coincides with the AUT's radiation origin. Classically and as suggested in [11], the phase center has been considered to be the radiation origin. Its definition, however, is not necessarily unique or applicable to every given radiating object. For the scope of this paper, the used definition of phase center is the one of radiation center suggested in [12], namely the point described by $\bar{r} = \bar{r}_{\text{PC}}$ for which $B_{\min} < B$ is the smallest possible so that

$$P_{\text{rad}, B_{\min}, \bar{r}_{\text{PC}}} = \frac{1}{2} \sum_{s=1}^{2} \sum_{l=1}^{B_{\min}} \sum_{m=-l}^{l} |T_{slm, \bar{r}_{\text{PC}}}|^2 \quad (7)$$
$$> P_{\text{rad}, B_{\min}, \bar{r}_i}, \quad \forall \bar{r}_i \neq \bar{r}_{\text{PC}}.$$

Qualitatively speaking, the power in the lowest modes for an expansion centered in $\bar{r}_{\text{PC}}$ is the most concentrated, causing any possible AUT displacement a power migration to higher regions of the spectrum.

In this paper, following assumptions are made:

- Sparsity is defined as how many terms of the SMC vector are zero.
- Assuming an expansion centered in $\bar{r}_{\text{PC}}$, the sparsity of the T_{slm} is highest for electrically symmetric or antisymmetric AUTs when they are oriented in a way that aligns their plane of symmetry to a plane of the expansion's coordinate system.
- For antennas with a well-defined main lobe and electrical symmetry, the sparsity is highest for an alignment of this lobe with the expansion's z-axis which also complies with the previous condition.

B. Coherence and Sampling Matrix

In compressed sensing, the sampling matrix must satisfy certain properties to guarantee robust recovery of sparse signals. One of these properties, namely Restricted Isometry Property (RIP), was introduced in the seminal papers on compressed sensing [13]–[15] and it was shown to be satisfied by random matrices drawn from a class of distributions. For many practical applications, the random sampling is not desirable and therefore deterministic sampling patterns should

be employed. However, it is NP-hard to certify whether a deterministic sampling matrix satisfies the RIP [16], [17] and therefore, another computationally tractable metric should be considered. In this work, we adopt the mutual coherence as the Fig. of merit. Roughly, the sampling matrices with high coherence are more prone to degraded recovery performance. Assuming the matrix of the spherical wave expansion $\mathbf{\Psi} = (\boldsymbol{\psi}_1, \boldsymbol{\psi}_2, \ldots, \boldsymbol{\psi}_N) \in \mathbb{C}^{M \times N}$, the coherence of a matrix $\mathbf{\Psi}$ is defined as

$$\mu(\mathbf{\Psi}) = \max_{i \neq j} \frac{|\langle \boldsymbol{\psi}_i, \boldsymbol{\psi}_j \rangle|}{\|\boldsymbol{\psi}_i\|_2 \|\boldsymbol{\psi}_j\|_2}. \qquad (8)$$

The coherence is lower bounded by the so called Welch bound, defined in context of correlation measurements of different signals [18], given as

$$\mu(\mathbf{A}) \geq \sqrt{\frac{N - M}{M(N - 1)}}. \qquad (9)$$

The bound is difficult to achieve for arbitrary pairs of M and N [19]. In this paper, the low coherence property is used as a metric to design a sampling matrix. A proposed sampling pattern over a sphere that could minimize the coherence of a SWE's sampling matrix is also discussed. In addition, the l_1-minimization or basis pursuit is used to recover the sparse signal $\boldsymbol{q} \in \mathbb{C}^N$

$$\min_{\boldsymbol{q}} \ \|\boldsymbol{q}\|_1 \ \text{ s.t } \ \boldsymbol{w} = \mathbf{\Psi}\boldsymbol{q}. \qquad (10)$$

III. A Compressed Sampling Scheme

In [20], the authors discussed how one can minimize the coherence for SH by considering only one inner product of two columns. In this section, this result of [20] is utilized. SH can be seen as a special case of SWE when the polarization is not taken into account. It can be proven that a specific class of sampling patterns, including equiangular sampling patterns, leads to high correlation between arbitrary columns of the sampling matrix. The equiangular sampling pattern for elevation θ and azimuth ϕ is described by

$$\phi_{p,j} = \frac{(p-1)\pi}{M-1}, \quad \theta_{p,j} = \frac{(j-1)2\pi}{M-1} \\ \text{for } p, j \in [1, 2, \ldots, M]. \qquad (11)$$

This scheme delivers a high coherence sampling matrix and, therefore, a poor recovery performance of the sparse signal. In addition, the authors also discuss the lower bound of the coherence of SH sampling matrices, where the lower bound is given by the product of Legendre polynomials $P_l(\cos\theta)$ with the highest degree. This means that, assuming a signal with bandwidth B and a degree from $0 \leq l \leq B - 1$, the lower bound is given by [20]

$$\mu(\mathbf{A}) \geq \sum_{p=1}^{M} P_{B-1}(\cos\theta_p) P_{B-3}(\cos\theta_p). \qquad (12)$$

This lower bound is not contrived, since a sampling pattern that achieves it does exist. For this case, a sampling pattern on elevation θ is considered with the following distribution

$$\cos(\theta_p) = \frac{2p - M - 1}{M - 1} \text{ for } p \in [1, 2, \ldots, M]. \qquad (13)$$

With a simple search algorithm, there is a corresponding pair on azimuth ϕ that can achieve the lower bound. In this case, the halting criterion is this lower bound. The algorithm is described below. Fig. 1 shows the distribution

---

Algorithm 1 Pattern search

Initialization : $\boldsymbol{\theta}, \boldsymbol{\phi}_0 \in \mathbb{R}^m$ as initial points, $\Delta_0 > 0$ as initial step size, standard basis $\boldsymbol{e}_i$ for $i \in [m]$, $\lambda \in (0, 1)$
for $k = 0, 1, \ldots$ until *halting criterion* **do**
  if $\mu(\boldsymbol{\theta}, \boldsymbol{x}) < \mu(\boldsymbol{\theta}, \boldsymbol{\phi}_k)$ for $\boldsymbol{x} \in S_k := \{\boldsymbol{\phi}_k \pm \Delta_k \boldsymbol{e}_i\}$ **then**
    $\boldsymbol{\phi}_{k+1} = \boldsymbol{x} \mod 2\pi$
    $\Delta_{k+1} = \Delta_k$
  else
    $\boldsymbol{\phi}_{k+1} = \boldsymbol{\phi}_k \mod 2\pi$
    $\Delta_{k+1} = \lambda \Delta_k$
  end if
end for

---

of the proposed sampling scheme for different numbers of total measurement points. It has been shown in [20] that the proposed sampling scheme enables a lower coherence property of the sampling matrix in comparison to other well-known sampling patterns, including equiangular, spiral, Hammersley and Fibonacci distributions. Moreover, it has been shown that the proposed scheme delivers a better recovery of sparse coefficients by using l_1 - minimization or basis pursuit. This proposed sampling strategy is applied to estimate the SMC from SNF measurements, whose reconstruction is then evaluated also in terms of the recovered far-field pattern for several antennas. This sampling scheme does not require two different polarizations to be measured at each proposed point and instead alternates two $90°$ rotated polarizations sequentially along ϕ.
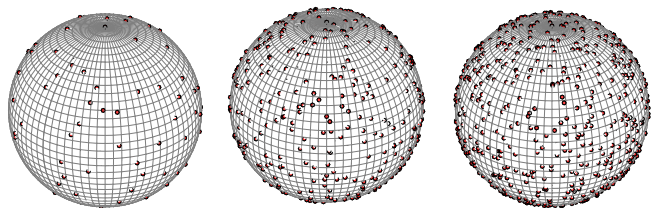
Fig. 1: Proposed sampling ($M = 97, M = 500, M = 800$).

IV. Reconstruction with Simulated Data

In this section, the recovery of SMC for three radiating structures is presented, namely a Hertzian dipole with off-set $x = \lambda/2$, an array of 3 z-directed dipole antennas, and a circular horn antenna. All three radiating structures are simulated for a design frequency of $f = 10\,\text{GHz}$. For these simulations, all antennas have been centered in the phase center according to the aforementioned definition to enhance sparsity [12], the offset of the dipole being applied afterwards. In addition, the SPGL1 method [21] is used as the basis pursuit

framework to recover the SMC. After estimating the SMC, the reconstructed far-field pattern of the antennas is shown in Fig. 2. The number of measurement points that is required for this reconstruction is $M < 0.2N$ for each case, which is less than 10 % of the amount of samples taken with conventional equiangular sampling, for which $M > 2N$. Having the

(a) Dipole   (b) Dipole Array   (c) Circular Horn
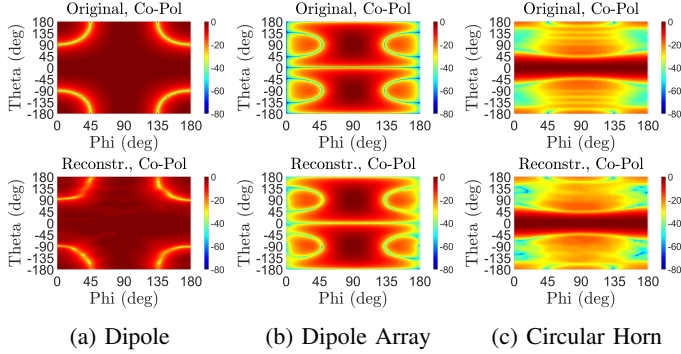
Fig. 2: Original co-polar component of the normalized far-field radiation pattern of all simulated antennas and their reconstruction using the proposed method.

circular horn the largest number of modes N among the three structures, its results are further analyzed. Since the theoretical cross-polarization component of an ideal horn along the main cuts $\phi = 0°$ and $\phi = 90°$ is zero, the reconstruction delivers a larger cross-polarization error for these cuts. To better observe the realized error for normal numerical cases, the cut $\phi = 45°$ is shown alongside the main cut $\phi = 0°$ in Fig. 3. The maximum and mean error curves for each theta cut calculated as the absolute difference of both normalized radiation patterns is shown in Fig. 4. It is shown hereby that the proposed sampling strategy reconstructs the far-field pattern needing fewer measurement points with an error lower than $-25\,\mathrm{dB}$ for the whole pattern and both polarizations.

V. Reconstruction with Measured Data

In this section, the described method is applied to a real measurement. The AUT is a double ridge guide horn antenna (AH Systems' SAS-571) and the measurement is performed at 10 GHz. To test the validity of the method for measurement data without entering in practical measurement considerations, the data is taken from a measurement performed with classical equiangular sampling. From the SMC calculated from this data, the measurement points under test are calculated according to the proposed sampling grid. The original measurement was performed for $M = 8784$ while the reconstruction is done for $M = 400$, which is $M < 0.06N$ and less than 3 % of the points needed for the equiangular sampling approach.

A. Reconstructed Data

After reconstructing the SMC with the proposed method, the far-field pattern of the antenna is reconstructed as seen in Fig. 5. A comparison between the original and reconstructed main cuts is highlighted by Fig. 7.
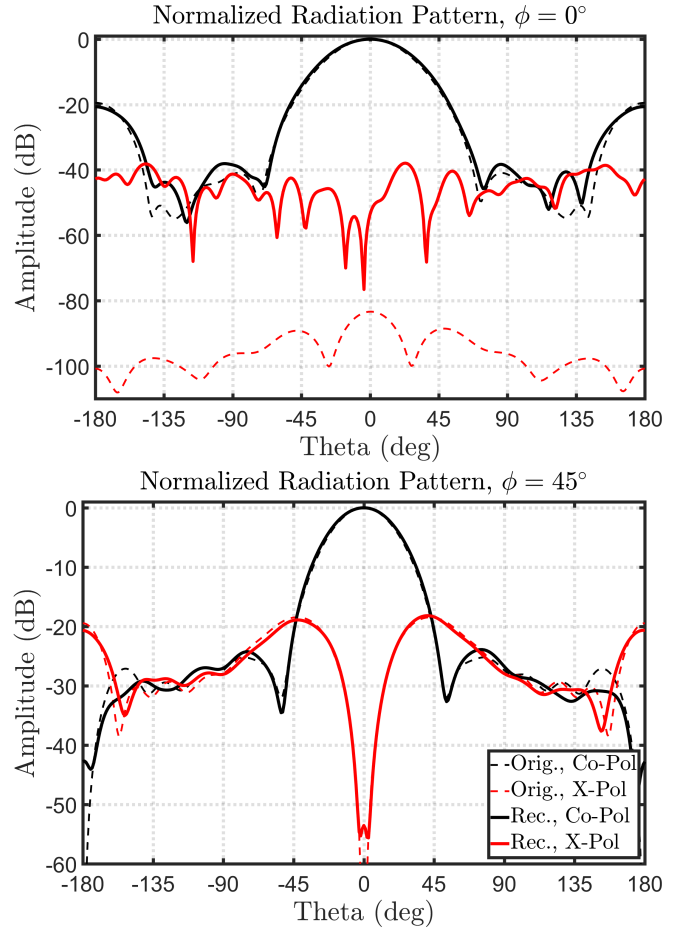
Fig. 3: The simulated horn's original normalized far-field radiation pattern and the pattern reconstructed with the proposed method.
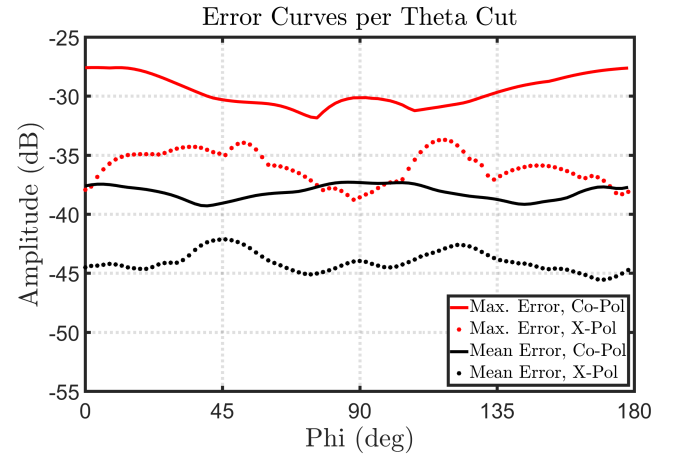
Fig. 4: Maximum and mean error curves calculated over each theta cut with a resolution of $\phi_{\mathrm{res}} = 2°$ for the simulated horn's reconstructed normalized far-field pattern.

The SMC estimated from the original measurement data and from the data matched to the proposed sampling scheme are shown in Fig. 8. It can be observed that the lowest modes i.e. the modes with the highest power content are reconstructed
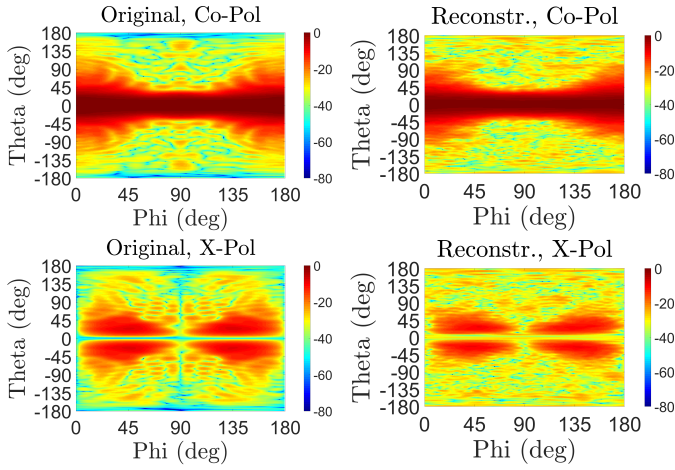
Fig. 5: 2D representation of the SAS-571's original normalized far-field radiation pattern and the pattern reconstructed with the proposed method.

the most successfully. The error curves are calculated in the same fashion as for the simulated data, i.e. as maximum and mean error per theta cut and are shown in Fig. 9. The global maximum error is $-15.6\,\text{dB}$, the global mean error is $-25.9\,\text{dB}$.

(a) $M = 97$ (b) $M = 400$
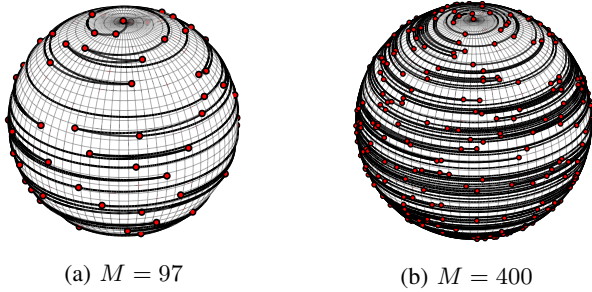
Fig. 6: Proposed sampling path for the proposed scheme.

B. Suggested Sampling Strategy and Estimated Measurement Time

In an equiangular-sampled measurement, the chamber's positioner is typically set up to have a continuous axis and a discrete or step axis. In this way, all points in each theta cut are acquired with a single sweep i.e., positioner rotation, needing to halt and rotate the phi axis by one resolution step between theta cuts. With the proposed sampling grid, more phi positions are needed but the movements on the continuous axis need not be complete turns, as shown in Fig. 6. For simplicity, a similar first approach is suggested. The shorter rotations reduce the time between movements in the step axis, thus decreasing the required measurement time per cut. Assuming the rotation after each resolution step in phi is done in the direction that provides the shortest path, the total rotation path for the proposed scheme is calculated. Adding the estimated time for the discrete steps, this time is compared to the measurement time needed for a classical equiangular measurement, assuming the same measurement speed for all axes and for both measurements. The estimated
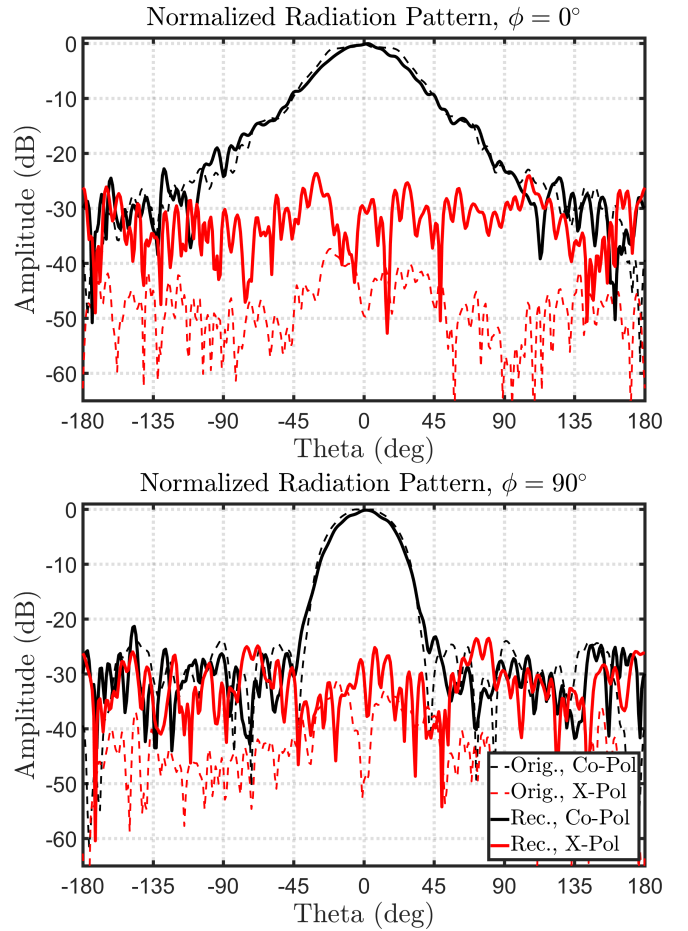
Fig. 7: SAS-571 original normalized far-field radiation pattern and the pattern reconstructed with the proposed method for $\phi = 0°$ and $\phi = 90°$.

(a) Original SMC   (b) Reconstructed SMC
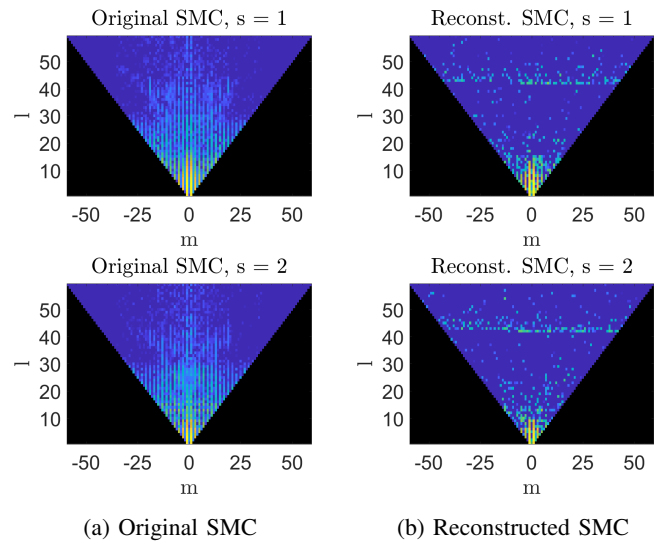
Fig. 8: SAS-571's original SMC and the SMC reconstructed with the proposed method.

speed increase with respect to a classical equiangular sampling is around $250\,\%$, i.e., the measurement time is slightly less
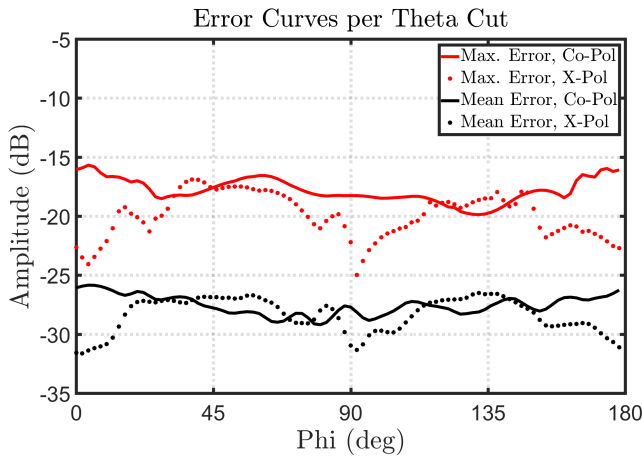
Fig. 9: Maximum and mean error curves calculated over each theta cut with a resolution of $\phi_{\mathrm{res}} = 2°$ of the SAS-571's reconstructed normalized far-field pattern.

than 40 % of the time needed for an equiangular measurement. For an increase of the measurement sphere's size, the number of sampling points of an equiangular measurement increase quadratically. However, most of these points are taken in the continuous rotations, thus not contributing to the increase of the measurement time. On the other hand, increasing the number of sampling points taken with the proposed sampling scheme linearly adds discrete steps. This results in a decrease of speed of the proposed sampling for larger antennas. As a comparison, a measurement for the proposed simulated circular horn using the proposed sampling scheme would increase the measurement speed by around 310 % with respect to an equiangular measurement, while a measurement of the dipole would be 390 % faster.

VI. SUMMARY AND FUTURE WORK

A novel compressed sampling scheme based on minimal coherence of the sampling matrix is introduced. The SMC of simulated and measurement data sampled with it are reconstructed using SPGL1 and the results are presented. The mean reconstruction error for the analyzed measurement data is $-25.9\,\mathrm{dB}$. The amount of sampling points considered is less than 3 % of the amount required for a measurement applying an equiangular sampling scheme.

The development of a compressed-sensing solver that implements *a priori* information of the SH, such as structural group sparsity, can improve the reconstruction error. The measurement can be further sped up by developing a more efficient scanning path for the given grid. Moreover, a method to determine the optimal number of measurement points M must be found. The limits of such method and the validity for radiating structures that do not comply with the presented SMC sparsity assumptions must be tested, together with the error introduced by basis mismatch.

ACKNOWLEDGEMENT

REFERENCES

[1] J. E. Hansen, *Spherical near-field antenna measurements*. IET, 1988, vol. 26.

[2] A. D. Yaghjian, "An overview of near-field antenna measurements," *IEEE Transactions on Antennas and Propagation*, vol. 34, no. 1, pp. 30–45, 1986.

[3] O. M. Bucci and C. Gennarelli, "Optimal interpolation of radiated fields over a sphere," *IEEE Transactions on Antennas and Propagation*, pp. 1633–1643, 1991.

[4] R. Cornelius and D. Heberling, "Analysis of sampling grids for spherical near-field antenna measurements," in *Progress in Electromagnetics Research Symposium (PIERS)*, 2015, pp. 923–927.

[5] T. K. Sarkar and A. Taaghol, "Near-field to near/far-field transformation for arbitrary near-field geometry utilizing an equivalent electric current and mom," *IEEE Transactions on Antennas and Propagation*, pp. 566–573, 1999.

[6] O. M. Bucci, C. Gennarelli, and F. D'Agostino, "A new and efficient nf-ff transformation with spherical spiral scanning," in *IEEE Antennas and Propagation Society International Symposium*. IEEE, 2001, pp. 629–632.

[7] R. Cornelius, A. A. Bangun, and D. Heberling, "Investigation of different matrix solver for spherical near-field to far-field transformation," in *9th European Conference on Antennas and Propagation (EuCAP)*. IEEE, 2015, pp. 1–4.

[8] B. Fuchs, L. Le Coq, S. Rondineau, and M. D. Migliore, "Fast antenna far field characterization via sparse spherical harmonic expansion," *IEEE Transactions on Antennas and Propagation*, vol. 65, no. 10, pp. 5503–5510, 2017.

[9] B. Fuchs, L. LeCoq, S. Rondineau, and M. D. Migliore, "Compressive sensing approach for fast antenna far field characterization," in *12th European Conference on Antennas and Propagation (EuCAP)*. IEEE, 2018.

[10] R. Cornelius, D. Heberling, N. Koep, A. Behboodi, and R. Mathar, "Compressed sensing applied to spherical near-field to far-field transformation," in *10th European Conference on Antennas and Propagation (EuCAP)*. IEEE, 2016, pp. 1–4.

[11] D. Löschenbrand and C. Mecklenbräuker, "Fast antenna characterization via a sparse spherical multipole expansion," in *2016 4th Int. Workshop on Compressed Sensing on Radar, Sonar, and Remote Sensing (CoSeRa)*. IEEE, 2016, pp. 212–16.

[12] C. Culotta-López, K. Wu, and D. Heberling, "Radiation center estimation from near-field data using a direct and an iterative approach," in *Antenna Measurement Techniques Association Symposium (AMTA)*. IEEE, 2017, pp. 303–308.

[13] E. J. Candès and T. Tao, "Near-optimal signal recovery from random projections: universal encoding strategies?" *IEEE Transactions on Information Theory*, vol. 52, no. 12, pp. 5406–5425, Dec. 2006.

[14] E. J. Candès, J. Romberg, and T. Tao, "Robust uncertainty principles: Exact signal reconstruction from highly incomplete frequency information," *IEEE Transactions on Information Theory*, vol. 52, no. 2, pp. 489–509, 2006.

[15] E. J. Candès and T. Tao, "Decoding by linear programming," *IEEE Transactions on Information Theory*, vol. 51, no. 12, pp. 4203–4215, 2005.

[16] A. M. Tillmann and M. E. Pfetsch, "The computational complexity of the restricted isometry property, the nullspace property, and related concepts in compressed sensing," *Information Theory, IEEE Transactions on*, vol. 60, no. 2, pp. 1248–1259, 2014.

[17] A. S. Bandeira, E. Dobriban, D. G. Mixon, and W. F. Sawin, "Certifying the restricted isometry property is hard," *IEEE transactions on information theory*, vol. 59, no. 6, pp. 3448–3450, 2013.

[18] L. Welch, "Lower bounds on the maximum cross correlation of signals (corresp.)," *IEEE Transactions on Information theory*, vol. 20, no. 3, pp. 397–399, 1974.

[19] M. Fickus and D. G. Mixon, "Tables of the existence of equiangular tight frames," *arXiv preprint arXiv:1504.00253*, 2015.

[20] A. Bangun, A. Behboodi, and R. Mathar, "Coherence bounds for sensing matrices in spherical harmonics expansion," in *IEEE International Conference on Acoustics, Speech and Signal Processing (ICASSP) 2018*. IEEE, 2018, p. has been accepted.

[21] E. van den Berg and M. P. Friedlander, "Spgl1: A solver for large-scale sparse reconstruction," 2007.